

Chapter 2

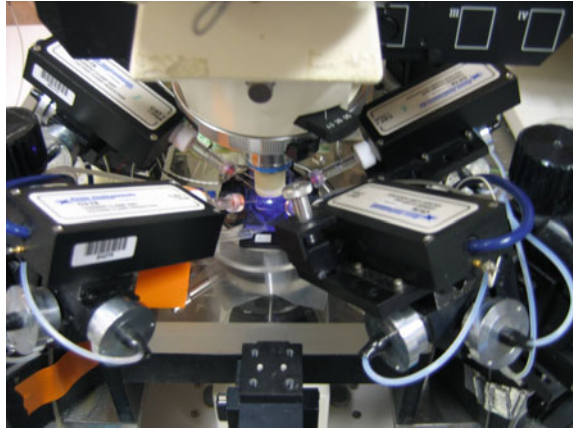
Bio-Electronics Interfaces

The so-called *bio-electronic field* has its roots in the late 18th century, with the famous experiments of Italian physicists Luigi Galvani and Giovanni Aldini on what at that time was called *animal bioelectricity* [1]. After these pioneering studies, the academic world had to wait about 150 years for the most important step ahead in this field. In fact, in the early '50s of the last century, Alan Lloyd Hodgkin and Andrew Huxley laid the foundation of modern electrophysiology with their groundbreaking work on the modeling of action potentials propagation in the squid's giant axon [2]. Starting from that point, the advances in the fabrication techniques allowed the realization of glass microelectrodes [3] and the consequent development of the patch-clamp technique through which it was possible to resolve the current of a single membrane channel [4]: modern neuroscience was born.

During the following years, the patch-clamp turned out to be an incredibly powerful tool giving us a close insight on how the membrane ion channels work, allowing to exactly resolve the ionic currents flowing in and out the membrane of an excitable cell. However, despite its numerous features, this useful tool has a big limitation. In fact, with such a technique it is almost impossible to investigate more than few cells at the same time (as clearly depicted in Fig. 2.1). It means that, using patch-clamp, the dynamics of cell aggregates can not be resolved, and with the advent of modern neuroscience this approach became therefore limiting.

This chapter is dedicated to the way in which the technology has evolved during the last 40 years in order to reliably interface the peripheral and the central nervous system (PNS and CNS respectively). Particular attention will be drawn to the most used devices for the transduction of extracellular signals, namely the Micro Electrode Arrays (MEAs) and the Field Effect Devices (FEDs).

Fig. 2.1 Patch clamp.
Typical experimental setup



2.1 Micro Electrode Arrays

The study of the central nervous system with extracellular (glass or metal) micro-electrodes dates back to the '40s of the last century [5] and, thanks to the strong effort put in the study of innovative materials and techniques, it rapidly improved during the '50s and the '60s [6–9]; nevertheless, it's with the introduction of fabrication techniques coming from the integrated circuits field [10] that the concept of planar micro-electrode had the possibility to come out and rapidly grow [11, 12], thus marking the beginning of the *Micro Electrode Array era*. MEAs, at the moment, represent the gold standard for extracellular monitoring of electroactive cells aggregates because of their well consolidated transduction principle [13] and the possibility to record and electrically stimulate cells both *in vivo* and *in vitro*. Standard materials for MEAs fabrication are Pt, Au, Ir_x and Indium Thin Oxide (ITO) for the electrodes, and Si₃N₄ and EPON SU-8 and polyimide for the passivation layer. Another important peculiarity of the MEA approach is the possibility to perform-long term recordings (up to several months for *in vitro* applications), with high stability and good reliability.

Classic MEAs are typically embedded in glass substrates. Nevertheless, during the last years, several kinds of innovative materials have been investigated in order to realize mechanically flexible MEAs for both *in vivo* (such as polyimide based [14], 3D flexible MEAs [15], and all-polymer MEAs made of Poly(3,4-ethylenedioxythiophene) Polystyrene sulfonate—PEDOT:PSS, an organic semiconductor), and *in vitro* applications (such as for example Polydimethylsiloxane-based devices [16]). More recently, an interesting approach for an easy-to-fabricate Micro-electrode Array based on a conducting polymer has been proposed by Sessolo et al. [17]. The flexibility is a very important feature dealing with *bio-applications* because of the huge differences in terms of mechanical properties between intrinsically “*soft*” living tissues and conventional materials for recording electrodes. This mechanical

incompatibility is strongly related to the so-called foreign-body response (especially in vivo applications), and this undesired effect must be minimized in order to obtain reliable and long-lasting bio-electronic interfaces.

2.1.1 Metal-Electrolyte Interface

In order to deeply understand the mechanisms behind the extracellular transduction of an action potential by means of metallic microelectrodes, it is crucial to understand what happens at the electrode/electrolyte interface. Two different phenomena may happen when a metal electrode is put inside an electrolyte solution and connected to a voltage source: either a current will flow through the circuit (thus the potential at the electrode/electrolyte interface does not change by changing the voltage), or no current will flow through the circuit (in this case a charge separation at electrode/electrolyte is obtained and the surface potential will follow exactly the voltage source variations). According to these two possible behaviors, electrodes are classified in not polarizable (as in the first case) and polarizable (as in the second case). A schematic representation of this classification is shown in Fig. 2.2.

Of course, in real applications the distinction between polarizable and not polarizable electrodes is not as sharp as it is in theory (in fact, only mercury can be considered a perfect polarizable metal, and only in a limited range of polarizations). A generally accepted way to describe the behavior of an electrode in contact with an electrolyte is to model it as the parallel between a capacitor (which models the extent to which the electrode is polarizable) and a resistor (which takes into account the presence of faradic currents). The resulting impedance shall be as follows:

$$Z_{\omega} = \frac{R_{el}}{j\omega R_{el}C_{el} + 1}. \quad (2.1)$$

The charge situation at the metal/electrode interface in the case of polarizable electrodes (i.e. $R \rightarrow \infty$) is described by the electrical double layer (EDL) theory

Fig. 2.2 Graphic representation of the double nature of the electrode/electrolyte interface, modeled as a RC circuit. An electrode is considered not polarizable when $R \rightarrow 0$ (a), and polarizable when $R \rightarrow \infty$ (b)

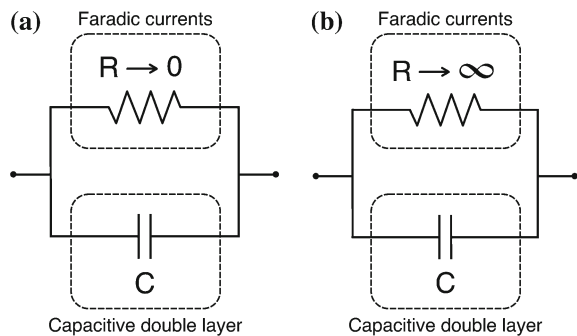
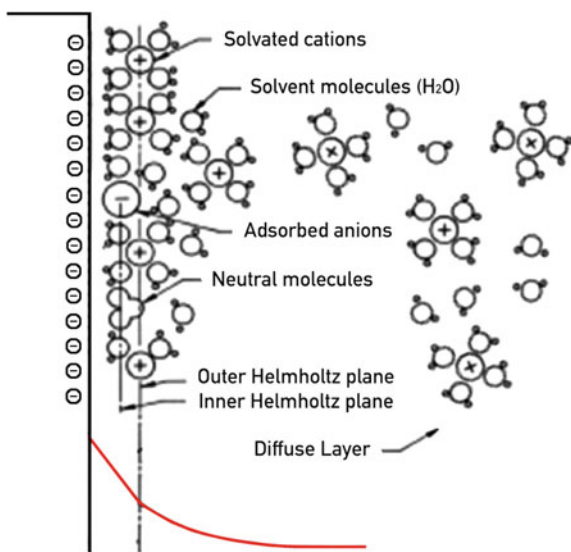
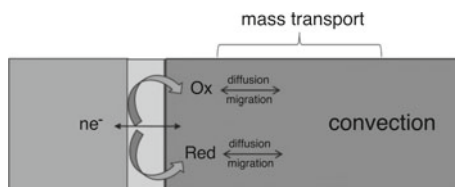


Fig. 2.3 Metal-electrolyte interface (Graham model) when the electrode is negatively biased. The potential evolution in the different layers is also shown (bottom trace)



proposed by Grahame in the late 40s [18]. According to the EDL theory, thanks to the electric field at the interface, charges (mainly bare ions, hydrated ions, and water molecules) in the electrolyte approach the electrode surface and form three distinct layers, each of which having different characteristics (as depicted in Fig. 2.3). The first plane is called inner Helmholtz plane (IHP) and is characterized by the presence of bare ions and small water dipoles; going toward the bulk of the solution, hydrated ions begin to aggregate and a second charge plane, called outer Helmholtz plane (OHP), is thus formed. The IHP and OHP are almost enough to compensate the charge in the metal. However, an additional amount of charge is located in the solution bulk, and this layer, which is needed to completely neutralize the metal charge, is called diffuse layer or *Gouy–Chapman* layer. As stated before, it is hard to obtain perfectly polarizable interfaces. In fact, faradic phenomena usually take place at the metal/electrolyte interface, due to redox reactions (see Fig. 2.4). Without any applied potential, the resulting net faradic current is zero, due to the fact that charge transport takes place at the same velocity in both directions, and it depends on the *equilibrium potential*. Out of equilibrium the dependence of the current to the applied potential

Fig. 2.4 Redox reactions at the electrode/electrolyte interface



is described by the *Butler–Volmer* equation:

$$I = A j_0 \left\{ \exp \left[\frac{\alpha n F}{RT} (E - E_{eq}) \right] - \exp \left[-\frac{(1 - \alpha) n F}{RT} (E - E_{eq}) \right] \right\} \quad (2.2)$$

where

- A : electrode area.
- j_0 : *exchange current density*. It represents the current upon equilibrium conditions.
- E : electrode potential.
- E_{eq} : equilibrium potential.
- T : absolute temperature.
- n : number of electrons involved in the redox reaction.
- α : *symmetry coefficient*.
- F and R : Faraday constant and universal gas constant.

For the sake of completeness, it is mandatory to specify that the Butler–Volmer equation does not consider mass transport effects (which are limited by the diffusion) from the bulk of the solution to the surface.

2.1.2 Cell/Planar Microelectrode Electrical Model

One of the strength points of the micro electrode approach is the relatively simple electrical model. The extracellular action potential transduction depends in fact only on few parameters with which it is possible to precisely control the cell/electrode coupling [19, 20] (for more information about the electrophysiological basis of action potentials, refer to Appendix C). In Fig. 2.5 a typical model for the neuron/planar

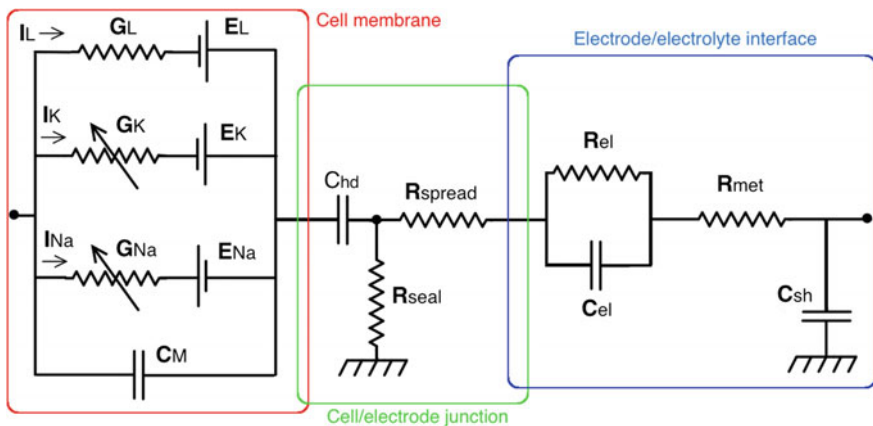


Fig. 2.5 Equivalent circuit of micro electrode-neuron interface. The cell membrane has been modeled as a Hodgkin-Huxley (HH) single compartment

microelectrode coupling is shown. By referring to Fig. 2.5 the parameters involved in the model are:

- C_{hd} is a capacitance made up of the series of the Helmholtz plane capacitance (C_h) and the Gouy–Chapman plane capacitance (C_d). Taking into account the dielectric constants of both planes (ϵ_{IHP} , ϵ_{OHP}) the following expressions for C_h and C_d are obtained:

$$C_h = \frac{(\epsilon_{IHP}\epsilon_0)(\epsilon_{OHP}\epsilon_0)}{(\epsilon_{IHP}\epsilon_0)d_{IHP} + (\epsilon_{OHP}\epsilon_0)d_{OHP}} A\delta$$

and

$$C_d = \frac{4q}{kT} \sqrt{\epsilon_d \epsilon_0 k T C_b} A\delta$$

where d_{IHP} e d_{OHP} are the Helmholtz planes thicknesses, ϵ_0 is the vacuum permittivity, A is the electrode area, and δ indicates the coverage percentage of the electrode.

- R_{seal} is the sealing resistance. It models the way in which the cell adhere to the electrode surface. For a planar electrode

$$R_{seal} = \frac{\rho_s}{d} \delta$$

where ρ_s is the electrolyte resistivity, d is the mean distance between cell and electrode, and δ indicates the coverage percentage of the electrode.

- R_{spread} is the spreading resistance. It is perpendicular to the cell membrane and the electrode surface and models the signal loss due to the cell-electrode distance. For circular, planar electrodes R_{spread} has the following expression:

$$R_{spread} = \frac{\rho_s \sqrt{\pi}}{4\sqrt{A_{electrode}}}.$$

Although MEAs are very powerful tools, they suffer from several drawbacks. The first one is related to the high costs associated to their production. In fact, the techniques and the materials employed to fabricate such devices are usually expensive, and this fact prevents the realization of, for example, disposable sensors. Another limitation is the need of an external reference electrode (usually an Ag/AgCl or a Pt electrode), which is generally bulky and limits the reduction of the device size. The difficulty to obtain high spatial resolution MEAs represents, as will be discussed later on in this chapter, another severe issue, and is mainly due to the external wiring that leads to the need of a complicated front-end electronics, which limits the number of recording sites to, typically, less than one hundred.

Another problem stems directly from the undesired redox reactions taking place at the cell-electrode interface during the electrical stimulation. As previously shown, the MEAs working principle strongly depends on the presence of the double layer

capacitance, which determines a capacitive coupling. Nevertheless, especially during stimulation trials (during which high levels of charge injection are needed in order to elicit a cellular action potential), unwanted faradic reactions may take place [21]. These faradic currents lead to a gradual degradation of the electrode (mainly because of corrosion) and may induce undesired biological response, such as membrane electroporation, or even cause water electrolysis.

2.2 Field Effect Devices for Electrophysiological Application

A different approach to extracellular measurements stems from the silicon technology. The introduction of an integrated-circuit approach to microelectrodes in 1970 [10] marked the beginning of a new paradigm in the way to interface the living matter. In the same year, Bergveld, with his famous letter [22], first proposed a completely new device for neurophysiological measurements called Ion Sensitive Field Effect Transistor. The full paper on the same topic was published two years later [23], and consolidated the ISFET theory, thus laying the foundation of a completely new field of research based on the exploitation of field effect devices for the transduction of extracellular biopotentials. In Fig. 2.6 an ISFET compared to a classic MOSFET is shown.

In the following years, tens of studies deepened the ISFET working mechanism and extended its applicability to different kinds of sensing applications (since, as Bergveld himself further confirmed, the ISFET device was specifically conceived as an electrophysiological tool), from cell metabolism monitoring both in vitro [24, 25] and in vivo [26] to the sensing of different enzymes [27] and ions concentration. The remarkable versatility (which is mainly due to the fact that the sensitivity

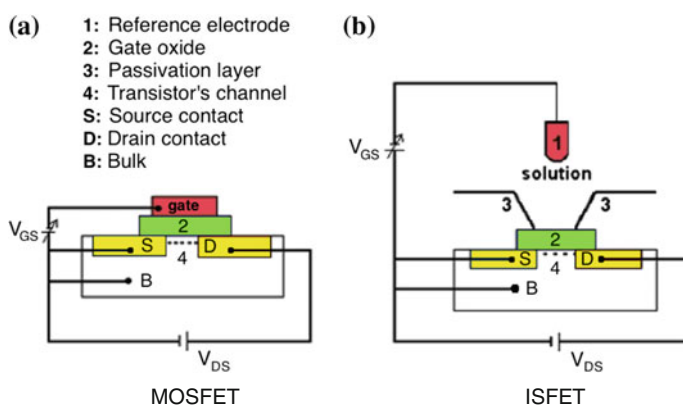


Fig. 2.6 Comparison between a classic MOSFET (a) and an ISFET (b). In ISFETs, the gate contact is replaced by the series of a metal electrode and an electrolyte

of an ISFET device depends on the composition of the oxide or on the species immobilized on the top of the gate area) allowed obtaining also heparin sensors [28], urea sensors, and glucose sensors [29, 30].

2.2.1 ISFET Transduction Principle

Despite ISFET's countless applications, its electrical behavior found a relatively simple characterization in classic MOSFET equations, since, as a matter of fact, it is nothing more than a MOSFET in which the gate metallization is replaced by the series of a reference electrode and an electrolyte (the bare gate oxide is directly exposed to the aqueous environment).

The general expression of the ISFET output current I_{DS} is, therefore, the same used for common MOSFETs. For a n-type device the I_{DS} is given by:

$$I_{DS} = C_{ox} \mu \frac{W}{L} \left[(V_{GS} - V_{TH}) V_{DS} - \frac{1}{2} V_{DS}^2 \right] \quad (2.3)$$

where C_{ox} is the capacitance of the gate oxide, μ is the charge carriers mobility, W and L are the channel width and length respectively. The threshold voltage has the following expression:

$$V_{TH} = V_{FB} - \frac{Q_B}{C_{ox}} + 2\phi_f \quad (2.4)$$

where V_{FB} is the flat-band voltage, Q_B is the depletion charge in the silicon and ϕ_f is the fermi-potential. The last term determines the onset of inversion and it depends on the doping level of the silicon. The flat-band voltage is a very important term in the definition of the working principle of a semiconductor device and can be expressed as

$$V_{FB} = \frac{\Phi_M - \Phi_{Si}}{q} - \frac{Q_{SS} - Q_{ox}}{C_{ox}} \quad (2.5)$$

where Φ_M and Φ_{Si} are the metal and the silicon workfunction respectively, Q_{SS} is the charge density at the silicon-oxide interface, and Q_{ox} is the fixed oxide charge.

Unlike classic MOSFETs, in which V_{TH} is a constant device property that depends on several process parameters and materials properties, in ISFETs its modulation is responsible for the pH sensitivity of the device. In fact, the expression of the ISFET threshold voltage contains additional terms that reflect the interface between the liquid and the reference electrode (E_{ref} , which contains Φ_M) and between the liquid and the gate oxide. The latter itself consists of two terms: χ_{sol} , which is the dipole potential of the solution, and Ψ_{eo} , which is called *surface potential* and results from a chemical reaction, governed by the dissociation of oxide surface groups (as it will be explained later on in this section). The resulting expression for the ISFET flat-band voltage is then

$$V_{FB} = E_{ref} - \Psi_{eo} + \chi_{sol} - \frac{\phi_{Si}}{q} - \frac{Q_{SS} + Q_{ox}}{C_{ox}} \quad (2.6)$$

To summarize:

- E_{ref} is the potential of the reference electrode with respect to the vacuum (it is obtained by summing up 4.7 V to the potential of the electrode with respect to the hydrogen standard electrode).
- ϕ_{Si} is the silicon workfunction.
- ϕ_M is the metal workfunction.
- Ψ_{eo} is the potential drop (with respect to the reference electrode) at the interface between the electrolyte and the insulator layer; this is the term of the equation that describes the pH sensitivity of the device and is determined by the interaction between H^+ ions and the insulator superficial groups.
- χ_{sol} is the (constant) potential due to the dipoles that are present in the liquid environment.
- Q_{SS} is the charge density at the silicon-oxide interface.
- Q_{ox} is the charge trapped inside the oxide layer.
- C_{ox} is the capacitance of the oxide.

As previously mentioned, the pH sensitivity of the ISFET depends on the term Ψ_{eo} , which in turn depends on the concentration of charged surface groups in the oxide. The role of these groups is explained by the so called *site-binding theory*, introduced by Yates et al. [31]. By considering the most general case of amphoteric surface groups [A-OH], it is possible to calculate the H^+ concentration at the surface:

$$[H_s^+] = \sqrt{\frac{K_a}{K_b} \frac{[A - OH_2^+]}{[A - O^-]}} \quad (2.7)$$

Due to the presence of a surface buffer capacity,¹ the bulk and the surface pH are not exactly the same. Using the Boltzmann equation it is possible to obtain the relation between the pH at the device oxide surface and its potential Ψ_{eo} :

$$[H_s^+] = [H_b^+] \exp\left[-q \frac{\varphi_{eo}}{kT}\right] \quad (2.8)$$

where $[H_b^+]$ is the bulk concentration of H^+ , k is the Boltzmann constant, T is the absolute temperature and q is the elementary charge. The φ_{eo} is then

$$\varphi_{eo} = 2.3 \frac{kT}{q} (pH_s - pH_b) \quad (2.9)$$

¹The buffer capacity is described as the concentration of strong acid/base to be added to the solution in order to obtain a given variation of surface pH.

and, given the buffer capacitance β and the surface differential capacitance C_s ² [32], the following expression for the device sensitivity is obtained:

$$\frac{d\varphi_{eo}}{dpH_b} = -2.3 \frac{kT}{q} \frac{1}{2.3 \frac{kT}{q^2} \frac{C_s}{\beta} + 1} = -2.3 \frac{kT}{q} \alpha \quad (2.10)$$

In 2.10, α is dimensionless and it varies between 0 and 1 depending on β and C_s , thus limiting the maximum sensitivity of an ISFET to a $2.3 \frac{kT}{q}$ mV/pH (~ 40 mV at room temperature for silicon dioxide).

2.2.2 ISFET-Based Sensors for Extracellular Monitoring of Excitable Cells: The Bergveld Model

The introduction of the ISFET within the scientific community changed irreversibly both bioelectronics and electrophysiology. In the specific case of extracellular recordings, ISFETs offer several advantages with respect to classic passive microelectrodes such as the absence of faradic currents due to the capacitive coupling between cells and the transistor channel, the precise control of size, geometry, and electrical properties of the device (thanks to the fabrication technology employed), and the possibility to interconnect many devices in array configurations [33]. This approach dramatically reduces the number of interconnections within the chip allowing to integrate more recording sites onto the same substrate.

The very first attempt of using a FET device in an *open-gate* configuration to the purpose of extracellular recording of electroactive cells activity was performed by Bergveld in the late '70s [34]. In the employed configuration, the cells (nerves or muscle fibers) are positioned onto the transistor gate oxide (a thin layer of silicon dioxide, which is biocompatible and provides a physical separation between the culture medium and the semiconductor). The device (called electrolyte-oxide-semiconductor FET, or EOSFET) differs from a classic ISFET, since the oxide surface is treated in order not to be hydrated. In this way, the extracellular signal can be treated as a small signal directly applied to the gate. Due to the almost ideal capacitive coupling, the spontaneous (or evoked) cell activity elicits a superficial variation of the channel conductivity, thus directly modulating the output current of the transistor.

As previously mentioned, this kind of cell/device interaction prevents charge transport phenomena, thus eliminating possible cell damaging effects (but also slowing down semiconductor degradation). Bergveld tested his device with invertebrate muscle cells, being able to record the evoked electrical activity of the tibial flexor of the hind leg of a locust. The employed transistor was an enhancement p-type FET and, as mentioned before, the oxide surface was treated in order to prevent its

²The differential capacity is the variation of superficial charge due to the variation of the potential at the interface between the insulator and the solution: $d\sigma_s/d\Psi_{eo}$.

hydration thus obtaining a quasi-ideal capacitive coupling between the cell and the semiconductor. In this way the device behaved almost exactly like a classic MOSFET.

The active surface of Bergveld's sensor is characterized by the presence of two distinct regions called *normal* and *parasitic* gate. The former region corresponds to the region between source and drain (called normal MOS transistor—MOST—or region G_1), while the latter is the external region (parasitic MOST, or region G_2). The drain current of the device is determined by the source-drain current of the normal MOST and by the contribution of the parasitic MOST, as described in Eq. 2.11 (g_1 and g_2 represent, respectively, the normal MOST, and the parasitic MOST gates):

$$I_d = \beta_1 (V_{g1} - V_{th}) V_d + \beta_2 (V_{g2} - V_{th}) V_d + (\beta_1 + \beta_2) \cdot \left[-\frac{1}{2} V_d^2 - \frac{2}{3} \alpha \{ (V_0 - V_b + V_d)^{3/2} \} \right] \quad (2.11)$$

where V_g is the gate potential, V_{th} is the device threshold voltage, and V_d and V_b are the potentials of the drain contact and of the bulk with respect to the source. The remaining parameters, α and β , reflect the I_{DS} dependence on the device geometry and on the semiconductor.

2.2.2.1 The OSFET Model

The theory behind the OSFET working principle comes from Rosenfalck studies, who calculated the potential distribution in a liquid medium due to the electrophysiological activity of nerve or muscle fibers (for more information, refer to [35]). Being the employed device a p-type enhancement transistor, during its operation, an inversion region is present at the semiconductor/oxide interface. Within this condition, the electrolyte/oxide/semiconductor junction may be conceived as a capacitor. More precisely, the capacitances C_1 and C_2 are associated, respectively, to the G_1 and G_2 regions. In order to derive the I_{ds} variations induced by potential changes in the electrolyte in close proximity to the device surface, it is convenient to split up C_1 and C_2 into n equivalent capacitors (C_1, C_2, \dots, C_n) having a common terminal on one side via the conducting inversion layer, and the other contact connected with different points in the conducting fluid in proximity to the oxide surface each having a known potential value (V_1, V_2, \dots, V_n) with respect to a point P in the bulk of the solution.

One of the most interesting feature of the Bergveld device is that, in principle, it may work in *floating mode*, i.e. without any reference electrode in the culture medium. By assuming that there is no connection to ground, there is no current flow through the external circuit. Furthermore, if the fluid where the OSFET is placed is uncharged, it is possible to sum up the initial charges Q_i at each capacity C_i caused by the corresponding potential V_i , thus obtaining the following charge conservation equation:

$$\sum_{i=1}^n Q_i = 0 \quad (2.12)$$

By applying the charge conservation principle stated in Eq. 2.12 to the expression of the potential across each capacitor and considering $n \rightarrow \infty$, the following expression for the electrolyte potential is obtained:

$$\frac{Q_i}{C_i} = V_i + V_P - V_S \quad (2.13)$$

$$V_P = -\frac{1}{A} \int \int_A V_i \delta A + V_S, \quad (2.14)$$

where $A = A_1 + A_2$ is the total oxide surface in contact with the electrolyte, and V_i is the potential difference between δA and P. As it can be noticed, the first element of the second part of Eq. 2.14 represents the mean potential difference V_i between the sensor surface and P.

As a result, the potentials $V_1 \dots V_n$ cause local variations inside the transistor channel. By expressing the mean potential of G_1 and G_2 regions as

$$V_{1,2}^* = \frac{1}{A_{1,2}} \int \int_A V_i dA$$

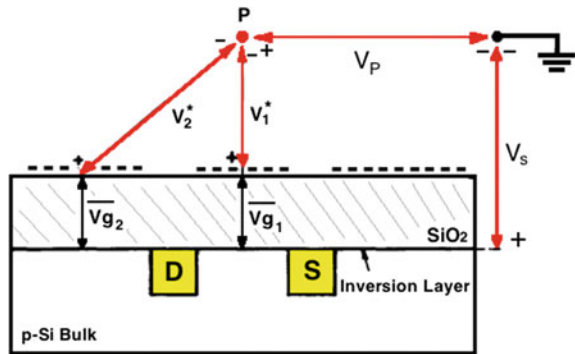
and by applying it to Eq. 2.14 is it possible to obtain

$$V_P = -\frac{A_1 V_1^* + A_2 V_2^*}{A} + V_S. \quad (2.15)$$

as outlined in the simplified model in Fig. 2.7. Therefore, the mean gate potentials of G_1 e G_2 can be expressed as

$$V_{g1,2} = V_{1,2} + V_P - V_S. \quad (2.16)$$

Fig. 2.7 OSFET model. Simplified model of the OSFET in contact with an electrolyte, in which the mean potentials V_1^* e V_2^* of, respectively, the normal and the parasitic MOST are generated



By substituting in the Eq. 2.16 the V_p expression previously obtained in 2.15, it is possible to obtain the following expressions for the gate potentials

$$\bar{V}_{g1} = \frac{C_2}{C_1 + C_2} (V_1^* - V_2^*) \quad (2.17)$$

$$\bar{V}_{g2} = \frac{C_1}{C_1 + C_2} (-V_1^* + V_2^*) \quad (2.18)$$

which model the electrolyte/OSFET interface for floating measurements. It is worth noting that the presence of a parasitic gate ($C_2 \neq 0$) in floating mode operation is needed in order to obtain a non-zero \bar{V}_{g1} . As a conclusion, from Eqs. 2.17 and 2.18 it is clear that \bar{V}_{g1} , and \bar{V}_{g2} are determined by the potentials across the capacities C_1 and C_2 due to the potential difference in the fluid $V_1^* - V_2^*$, which is expected to be generated by nerve (or muscle) bio-electric activity.

However, when the electrolyte is capacitively grounded, different expressions for Eqs. 2.17 and 2.18 are obtained

$$\bar{V}_{g1} = V_1^* - V_2^* - V_S \quad (2.19)$$

$$\bar{V}_{g2} = V_2^* - V_S \quad (2.20)$$

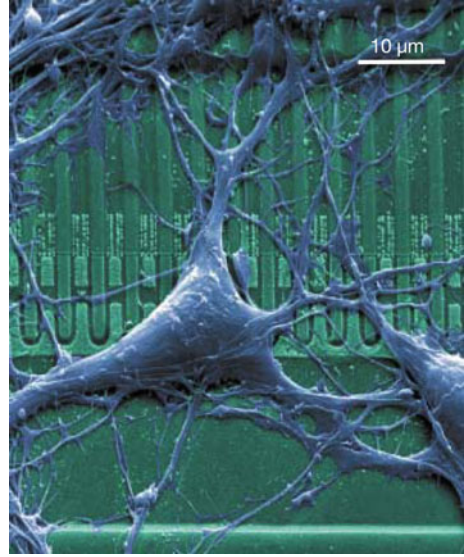
In the case modeled by 2.19 and 2.20, the OSFET behaves like a normal MOST, and the electrophysiological activity of a muscle cell may be measured extracellularly with respect to the reference electrode with which the electrolyte is grounded.

2.2.3 ISFET-Based Sensors for Extracellular Monitoring of Neurons Activity: The Fromherz Model

After the inspiring work of Bergveld on ISFETs and OSFETs, the interest in the employment of such devices in neurophysiological applications quickly grew up. Several groups around the world began to study different FET-based devices [36] and different animal models, such as invertebrate neurons [37]. A huge step forward in the integration of silicon devices to neuronal cells was reached in the early '90s of the last century by Peter Fromherz and its group [38] who proposed a very interesting model for the silicon/neuron coupling. In a very famous set of experiments, they coupled a leech neuron to the gate oxide of an n-type field effect transistor, and the cell's electrical activity was monitored simultaneously by a patch pipette and the transistor itself. This first pioneering work, together with subsequent works by the same group [39–43], helped to understand the nature of the coupling between cells and FET devices, both for recording and stimulation of the central nervous system. In Fig. 2.8, a rat hippocampal neuron cultured onto a FET array is shown.

In the following, the model proposed by Fromherz will be briefly discussed.

Fig. 2.8 Rat hippocampal neuron cultured onto a linear FET array in an *open-gate* configuration. Reprinted with permission from [44]. Copyright 2002, John Wiley and Sons



2.2.3.1 The Core-Coat Conductor

Considering a neuronal cell and a transistor in an open-gate configuration, their coupling should be a direct capacitive coupling. In this ideal situation, two dielectric layers, namely the lipid double layer and the oxide layer, separate two conductive materials, i.e. the intracellular medium on one side and the silicon on the other side, as depicted in Fig. 2.9a. A classic capacitor is then formed, and the cell electrical activity would be able to directly polarize the FET oxide, thus inducing an electric field variation and a subsequent modulation of the output current of the transistor. In turn, under these ideal conditions, a signal applied through the gate oxide will easily elicit an action potential, by acting on the voltage-gated ion channels in the cell membrane.

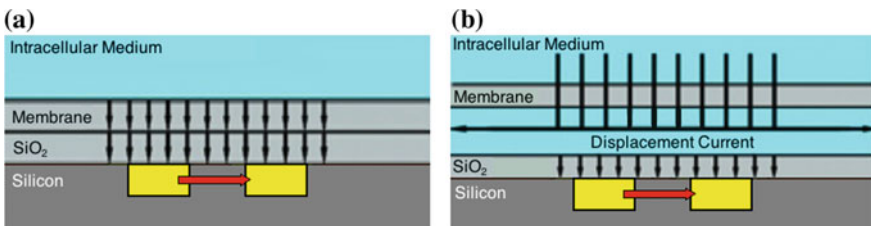


Fig. 2.9 Cell-silicon interface: **a** Ideal case: the FET oxide is directly polarized by the cell during an action potential. **b** Real case: the presence of a cleft filled with a small volume of culture medium transforms the ideal capacitive structure of the previous case in a core-coat structure

Unfortunately, the cell-FET coupling nature is quite different from the pre-mentioned scenario. The cell-FET coupling is in fact mediated by membrane proteins and/or protein layers adsorbed onto the oxide surface. The presence of these proteins mediators determines the formation of a cleft between the cell and the device. The presence of a conductive cleft (which is filled with extracellular medium) prevents the oxide (cell) to be directly polarized from the cell activity. This more realistic situation is depicted in Fig. 2.9b.

The resulting structure cannot be represented as an ideal capacitor anymore. The cell-FET coupling is more likely a *core-coat* structure, in which a thin conductive layer (the cleft) that represents the “core” is confined by the cell membrane and the oxide layer. Using the core-coat conductor theory, the transduction mechanism would rely on the propagation in the cleft of a *transductive extracellular potential* (TEP), which would modulate the electric field across the oxide thus affecting the output current of the transistor. The stimulation of the cell’s electrical activity through an open-gate FET would be easily described in terms of TEP as well. These phenomena are driven by two main events:

- The cell electrical activity (or a stimulus applied through the transistor’s open-gate) induces a displacement current through the cell membrane (or through the gate oxide) [45]. This current will induce a TEP inside the conductive cleft between the cell and the transistor [46].
- The TEP (either induced by the cell’s activity or by an impulse applied through the transistor’s open-gate) induces an electric field that can be sensed by the FET (as a modulation of its drain current) or by the cell (thanks to the presence, in the cell membrane, of voltage-dependent ionic channels).

Two models have been proposed and developed in order to explain the mechanism behind the TEP propagation in the cleft, namely the *area contact* model (ACM) and the *point contact* model (PCM). The two models differ from each other by their dimensionality: two-dimensions for the ACM and zero-dimensions for the PCM [46].

2.2.3.2 Area Contact Model

In this model, the current flowing inside the cleft is balanced from the displacement currents through the gate oxide and the cell membrane (as shown in Fig. 2.10a). The equation

$$-\nabla \left(\frac{1}{r_j} \nabla V_j \right) = c_s \left(\frac{\partial V_s}{\partial t} - \frac{\partial V_j}{\partial t} \right) + c_M \left(\frac{\partial V_M}{\partial t} - \frac{\partial V_j}{\partial t} \right) + g_{JM} (V_M - V_j) \quad (2.21)$$

represents the charge conservation (per unit area) when the electrolyte is grounded by means of a reference electrode ($V_E = 0$ V). The left-hand side of the Eq. 2.21 refers to the current (per unit length) balance in the cleft, while the right-hand side represents

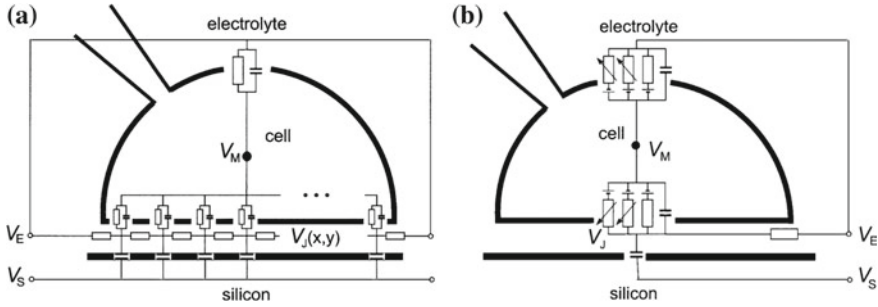


Fig. 2.10 Circuital models for **a** area contact model and **b** point contact model. Reprinted with permission from [47]. Copyright 2003, Elsevier

the current (per unit area) through the gate oxide and the cell membrane. V_M is the membrane potential, V_S is the voltage applied to the substrate (if any), V_J is the TEP in the junction, r_j is the cleft resistance (calculated as the ratio between the cleft specific resistance ρ_j and its thickness d_j), C_M and C_S are the specific capacitances (per unit area) respectively of the cell membrane and the substrate, and g_{JM} is the leakage area-specific conductance of the portion of the membrane in contact with the exposed gate oxide of the FET.

2.2.3.3 Point Contact Model

A more convenient approach to the TEP definition is to model the conductive cleft with a global conductance G_J and the cell membrane and the oxide layer with, respectively, a global capacitance C_{JM} and a global capacitance C_S [48], as depicted in Fig. 2.10b. Considering A_{JM} the superposition area between the cell membrane and the transistor, it is possible to define the following area-specific parameters: $c_M = C_M/A_{JM}$, $c_S = C_S/A_{JM}$, and $g_J = G_J/A_{JM}$. The resulting equation for the currents in the cleft will be as following

$$g_J (V_J - V_E) = c_S \left(\frac{dV_S}{dt} - \frac{dV_J}{dt} \right) + c_M \left(\frac{dV_M}{dt} - \frac{dV_J}{dt} \right) + \sum_i g_{JM}^i (V_M - V_J - V_0^i) \quad (2.22)$$

where $g_{JM}^i = G_{JM}^i/A_{JM}$ models the ion-selective conductances of membrane channels, and V_0^i is the inversion potential of the i th ion (which depends on the i th ion concentrations present in and out the cell membrane).

The TEP depends on the current variations inside the cleft only if V_M and V_S are externally imposed (it is possible to control V_M by means of patch clamp techniques). The situation changes a bit by considering a non-invasive measurement, in which

the V_M follows its own dynamics that depends on ions balancing and ionic currents through the cell membrane (both the cell membrane portion facing the FET and the “free” portion of the membrane, that is, the cell membrane facing the bulk of the culture medium). By applying the Kirchhoff law to the PCM equivalent circuit it is possible to obtain the following equation:

$$\begin{aligned} c_M \left(\frac{dV_M}{dt} - \frac{dV_E}{dt} \right) + \sum_i g_{FM}^i (V_M - V_E - V_0^i) \\ = -\beta_M \left[c_M \left(\frac{dV_M}{dt} - \frac{dV_E}{dt} \right) + \sum_i g_{JM}^i (V_M - V_E - V_0^i) \right] \end{aligned} \quad (2.23)$$

where the left hand side describes the current flowing out through the free portion of the membrane, while the right hand side models the current flowing inside the cell from the membrane that faces the transistor. The terms g_{JM} and g_{FM} represent the ionic conductances of the junction cell membrane and the free cell membrane respectively, and $\beta_M = A_{JM}/A_{FM}$ is the ratio between the areas of the pre-mentioned cell membrane portions.

2.2.4 Cell-FET Hybrids

Fromherz's studies opened up a completely new branch in the bioelectronic field. The possibility to realize real neuron-FET hybrids thrilled the scientific community, and in the following years a lot of effort was put on the development of new systems specifically tailored in order to let the living tissue communicate (bi-directionally) with silicon based devices.

The first attempt to reach the goal of a bi-directional system for neural communication dates back to 1997, with the work of Stett et al. [49]. A p-type transistor in an open-gate configuration was employed to record the neurons' activity, while a little spot of heavily p-doped silicon, insulated with a thin layer of thermally grown silicon oxide, placed in close proximity to the recording site, was employed for neural stimulation. The proposed hybrid circuit was therefore of a chip/neuron/chip kind, since the capacitive stimulation from the chip elicited the neuronal activity, and this neuronal activity was subsequently recorded using a device in the same chip (as shown in Fig. 2.11a). More precisely, the application of a stimulus V_S^0 from the stimulating spot, induced a TEP that can be modeled as follows:

$$V_J(t) = V_S^0 \frac{c_S}{c_S + c_M} \exp \left(-\frac{g_J}{c_S + c_M} t \right). \quad (2.24)$$

As an example, using the following parameters $V_S^0 = 3 \text{ V}$, $g_J = 30 \text{ mS/cm}^2$, $c_S = 0.34 \text{ } \mu\text{F/cm}^2$ e $c_M = 4 \text{ } \mu\text{F/cm}^2$, the resulting $V_J(t)$ will be equal to 230 mV with a time

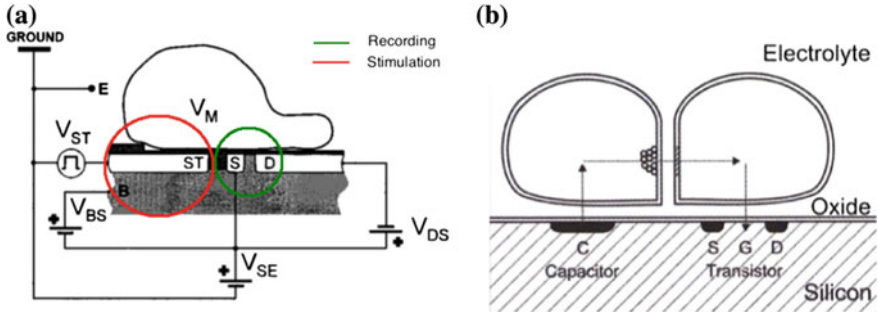


Fig. 2.11 **a** Chip/neuron/chip hybrid circuit. Reprinted with permission from [49]. Copyright 1997, American Physical Society. **b** Chip/neuron/neuron/chip hybrid circuit: a fast capacitive stimulation elicits a response (an action potential) in the cell marked as A; A's activity stimulates the cell marked as B (through a soma-soma interaction), and B's activity is recorded by the FET. Reprinted with permission from [40]. Copyright 2004, American Physical Society

constant equal to $110 \mu\text{s}$. This evoked TEP is enough to cause the depolarization of the cell membrane portion facing the stimulating spot, thus eliciting an action potential. It has been demonstrated that the previous stimulation mechanism cause no harm to the cell, though it may induce temporary electroporation of the cell membrane [40]. The evoked neuronal activity $V_M(t)$ will induce another TEP that can be recorded from the FET:

$$V_J(t) = \frac{1}{g_J} \left[c_M \frac{dV_M}{dt} + \sum_i g_{JM}^i (V_M - V_0^i) \right] \quad (2.25)$$

where g_{JM}^i and V_0^i are the membrane conductance and the reverse potential of the i th ion respectively. The bidirectional circuit to which the Eqs. 2.24 and 2.25 refer to, is shown in Fig. 2.11b. During the following years, several hybrid circuits have been studied, such as chip/neuron/neuron/chip [40] and neuron/chip/neuron circuits [50].

To summarize, the Fromherz model relies on the induction (either by the cell's electrical activity or by an impulse applied through the transistor's gate) of a transductive extracellular potential in the cleft between the cell and the transistor, which together form a core-coat conductor. A high TEP is related to high displacement currents along the cell membrane and along the gate oxide layer, and on the junction conductance (which should be as high as possible). Good recordings and stimulations of neuronal electrical activity are fostered by a little cleft width d_J , by a high specific resistance ρ_J , and by a high junction area. An effective recording needs high ionic conductances g_{JM}^i (in the membrane portion that face the FET), while a high oxide capacitance c_S facilitates an effective capacitive stimulation.

2.3 High-Density FEDs: The APS MEA

As previously extensively highlighted, MEAs constitute a very important tool in neuronal networks studies, since these kind of devices are able to perform long-term recordings on electroactive cells aggregates and to elicit responses through electrical stimulations, both in vivo and in vitro. During the last decades, lots of effort have been done to improve the performances of such devices. In particular, bioMEMs (bio Micro Electro-Mechanical systems) integration allowed the realization of more and more complex structures, such as the so-called *neuro-cages* [51], or particular micro-structures for neuronal networks patterning [52, 53].

Despite the enormous effort and the undeniable advances, classic MEAs still suffer from several drawbacks such as the high impedances (which limit the scale down of the recording sites), the current shielding phenomenon [54], and the difficult management of the external wiring, making it difficult to obtain high-density MEAs. For example, for a standard neuronal in vitro application, it is easy to have more than 50,000 neurons against up to few hundreds recording sites, and this results in a high spatial under-sampling of the culture's activity.

In order to overcome these problems, CMOS technology has been introduced in the realization of a new family of MEA devices with a high recording sites density and on-chip signal conditioning (such as, for example, pre-amplification stages, AD conversion, and multiplexing), thus reducing the external wiring complexity. Representative examples of a CMOS device for neurophysiological applications are the so called *Michigan probes* [55], a widely employed tool for in vivo applications, and the chip proposed by Heer et al. [56], which was able to record from 128 electrodes with a sampling frequency of up to 20 kHz. These two devices are showed in Fig. 2.12a, b.

Another interesting approach involving CMOS technology is the Active Pixel Sensor approach (APS—this method was originally conceived for video applications [57]). In 2005, Berdondini et al. [58] developed an APS-MEA for in vitro applications, consisting of 6464 pixels on an active surface of 2.5 mm × 2.5 mm.

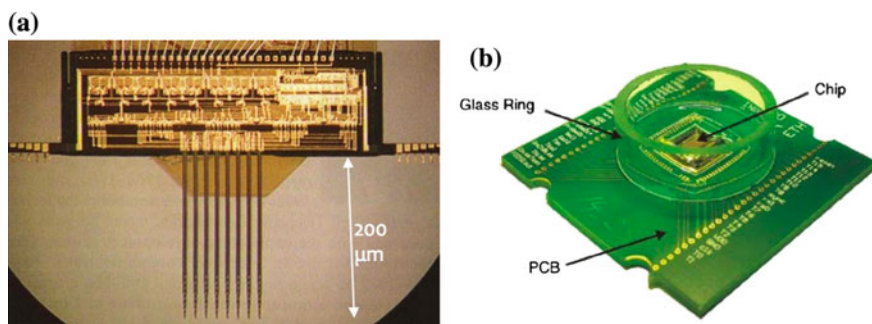
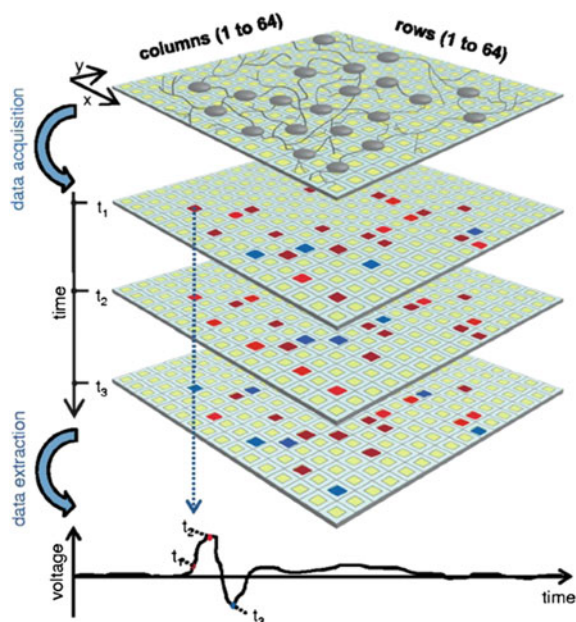


Fig. 2.12 **a** A 3D Michigan probe for in vivo. **b** A CMOS MEA for in vitro applications. The chip consisted of 128 addressable electrodes (sampling frequency: 20 kHz). Reprinted with permission from [56]. Copyright 2007, Elsevier

Fig. 2.13 APS-MEA working principle. Cells are cultured on the active surface of the device, and the electrophysiological signals are recorded as frame sequences. With this technique it is possible to visualize the overall cultures activity by simply coding the extracellular signals recorded by each electrode with a false color map. Reprinted with permission from [59]. Copyright 2009, Royal Society of Chemistry



Each pixel had a dimension of $40\mu\text{m} \times 40\mu\text{m}$, a microelectrode of $20\mu\text{m} \times 20\mu\text{m}$ and a low noise pre-amplifier ($11\mu\text{V}_{rms}$), resulting in an electrode separation of $20\mu\text{m}$. An important progress compared to other high density chip, was the possibility to address each pixel with a sampling frequency up to 125 kHz and a full-frame sampling frequency of 7.8 kHz. The on-chip pre-amplification allowed to simplify the external wiring and to perform a reliable on-board signal conditioning. Moreover, the APS approach, by exploiting video and image editing paradigms, offered a real time representation of the cellular activity with a temporal resolution up to $8\mu\text{s}/\text{pixel}$ for a 64 pixels subset [59]. The APS-MEA working mechanism is shown in Fig. 2.13.

2.4 Extended Gate Transistors for Electrophysiological Applications

Previously in this chapter, two important models of the FET-cell interface have been presented, namely the Bergveld model and the Fromherz model. Both of them describe the interaction between an electrogenic cell and a transistor in an *open-gate* configuration, which means that the cells are directly cultured onto the gate oxide of a transistor (no gate metallization is present). An alternative approach is represented by the employment of extended gate structures. This approach has, undoubtedly, several advantages with respect to the open-gate approach, since the transistors channels are physically separated from the culture region, and they can be thus properly

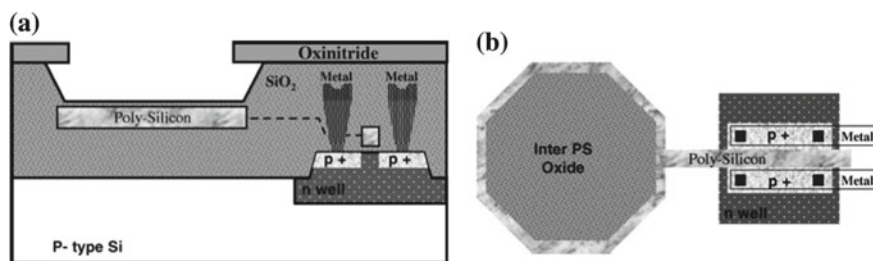


Fig. 2.14 Cross section (a) and top-view (b) of the extended gate device proposed by Cohen et al. Reprinted with permission from [63]. Copyright 2004, Elsevier

passivated in order to protect them against the light and against the harsh environment where the cells are cultured in. In extended gate transistors, each microelectrode can be either directly connected to the gate of a FET [60, 61] or realized using a floating gate approach [62]. In the last approach, the cells are cultured onto the thin insulation layer of an elongated gate that is left floating. As an example, in 2004 Cohen et al. [63] proposed an FGFET device for in vitro application consisting of a p-type transistor with an insulated poly-silicon gate (covered by 420 Å of thermally growth oxide) that acted as the recording site (Fig. 2.14a, b).

References

- Galvani, L., Aldini, G.: *De Viribus Electricitatis In Motu Musculari Comentariorum Cum Joannis Aldini Dissertatione Et Notis. Accesserunt Epistolae ad animalis electricitatis theoriam pertinentes* (Google eBook) (1792)
- Hodgkin, A.L., Huxley, A.F.: A quantitative description of membrane current and its application to conduction and excitation in nerve. *J. Physiol.* **117**, 500–544 (1952)
- Kennard, D.W.: Glass microcapillary electrodes used for measuring potential in living tissue. *Electronic Apparatus for Biological Research*, pp. 534–567. Butterworths, London (1958)
- Neher, E., Sakmann, B., Steinbach, J.H.: The extracellular patch clamp: a method for resolving currents through individual open channels in biological membranes. *Eur. J. Physiol.* **375**, 219–228 (1978)
- Renshaw, B., Forbes, A., Morison, B.R.: Activity of Isocortex and Hippocampus: Electrical studies with micro-electrodes. *J. Neurophysiol.* **3**(1), 74–105 (1940)
- Li, C.L., Jasper, H.: Microelectrode studies of the electrical activity of the cerebral cortex in the cat. *J. Physiol.* **121**, 117–140 (1952)
- Hubel, D.H.: Tungsten microelectrode for recording from single units. *Science* **125**, 549–550 (1957)
- Verzeano, M., Negishi, K.: Neuronal activity in cortical and thalamic networks a study with multiple microelectrodes. *J. Gen. Physiol.* **43**, 177–195 (1960)
- Guld, C.: A glass covered platinum microelectrode. *Med. Electron. Biol. Eng.* **2**, 317–327 (1964)
- Wise, K.D., Angell, J.B., Starr, A.: An integrated-circuit approach to extracellular microelectrodes. *IEEE Trans. Biomed. Eng.* **17**(3), 238–247 (1970)
- Thomas, C.A., Springer, P., Loeb, G., Berwaldnetter, Y., Okun, L.: A miniature microelectrode array to monitor the bioelectric activity of cultured cells. *Exp. Cell Res.* **74**(1), 61–66 (1972)

12. Gross, G.W., Rieske, E., Kreutzberg, G.W., Meyer, A.: A new fixed-array multi-microelectrode system designed for long-term monitoring of extracellular single unit neuronal activity in vitro. *Neurosci. Lett.* **6**(2–3), 101–105 (1977)
13. Bove, M., Grattarola, M., Martinoia, S., Verreschi, G.: Interfacing cultured neurons to planar substrate microelectrodes: characterization of the neuron-to-microelectrode junction. *Bioelectrochem. Bioenerg.* **38**(2), 255–265 (1995)
14. Rousche, P.J., Pellinen, D.S., Pivin, D.P., Williams, J.C., Vetter, R.J., Kipke, D.R.: Flexible polyimide-based intracortical electrode arrays with bioactive capability. *IEEE Trans. Bio-med. Eng.* **48**(3), 361–371 (2001)
15. Takeuchi, S., Suzuki, T., Mabuchi, K., Fujita, H.: 3D flexible multichannel neural probe array. *J. Micromech. Microeng.* **14**(1), 104–107 (2004)
16. Blau, A., Murr, A., Wolff, S., Sernagor, E., Medini, P., Iurilli, G., Ziegler, C., Benfenati, F.: Flexible, all-polymer microelectrode arrays for the capture of cardiac and neuronal signals. *Biomaterials* **32**(7), 1778–1786 (2011)
17. Sessolo, M., Khodagholy, D., Rivnay, J., Maddalena, F., Gleyzes, M., Steidl, E., Buisson, B., Malliaras, G.G.: Easy-to-fabricate conducting polymer microelectrode arrays. *Adv. Mater. (Deerfield Beach, Fla.)* **25**(15), 2135–2139 (2013)
18. Grahame, D.C.: The electrical double layer and the theory of electrocapillarity. *Chem. Rev.* **41**(3), 441–501 (1947)
19. Robinson, D.A.: The electrical properties of metal microelectrodes. *Proc. IEEE* **56**(6), 1065–1071 (1968)
20. Martinoia, S., Massobrio, P., Bove, M., Massobrio, G.: Cultured neurons coupled to microelectrode arrays: circuit models, simulations and experimental data. *IEEE Trans. Biomed. Eng.* **51**(5), 859–864 (2004)
21. Cogan, S.F.: Neural stimulation and recording electrodes. *Annu. Rev. Biomed. Eng.* **10**(1), 275–309 (2008)
22. Bergveld, P.: Development of an ion-sensitive solid-state device for neurophysiological measurements. *IEEE Trans. Biomed. Eng.* **BM17**(1), 70 (1970)
23. Bergveld, P.: Development, operation, and application of the tool for electrophysiology. *IEEE Trans. Biomed. Eng.* **19**(5), 342–351 (1972)
24. Baumann, W.H., Lehmann, M., Schwinde, A., Ehret, R., Brischwein, M., Wolf, B.: Microelectronic sensor system for microphysiological application on living cells. *Sens. Actuators B* **55**, 77–89 (1999)
25. Lehmann, M., Baumann, W., Brischwein, M., Ehret, R., Kraus, M., Schwinde, A., Bitzenhofer, M., Freund, I., Wolf, B.: Non-invasive measurement of cell membrane associated proton gradients by ion-sensitive field effect transistor arrays for microphysiological and bioelectronic applications. *Biosens. Bioelectron.* **15**(3–4), 117–124 (2000)
26. Shimada, K., Yano, M., Shibatani, K., Komoto, Y., Esashi, M., Matsuo, T.: Application of catheter-tip i. s. f. e. t. for continuous in vivo measurement. *Med. Biol. Eng. Comput.* **18**, 741–745 (1980)
27. van der Schoot, B.H., Bergveld, P.: ISFET based enzyme sensors. *Biosensors* **3**(3), 161–186 (1987)
28. Van Kerkhof, J.C., Bergveld, P.: The ISFET based heparin sensor with a monolayer of protamine as affinity ligand. *Biosens. Bioelectron.* **10**, 269–282 (1995)
29. Miyahara, Y., Moriizumi, T., Ichimura, K.: Integrated enzyme fets for simultaneous detections of urea and glucose. *Sens. Actuators* **7**(1), 1–10 (1985)
30. Byung-Ki, S., Byung-Woog, C., Chang-Soo, K., Dae-Hyuk, K.: ISFET glucose and sucrose sensors by using platinum and photo-crosslinkable polymers Kwon c. *Sens. Actuators B: Chem.* **41**, 2–6 (1997)
31. Yates, D.E., Levine, S., Healy, W.: Site-binding model of the electrical double layer at the oxide/water interface. *J. Chem. Soc. Faraday Trans. 1: Phys. Chem. Condens. Phases* **70**, 1807–1818 (1973)
32. van Hal, R.E.G., Eijkel, J.C.T., Bergveld, P.: A novel description of ISFET sensitivity with the buffer capacity and double-layer capacitance as key parameters. *Sens. Actuators B: Chem.* **24**, 201–205 (1995)

33. Feili, D., Schuettler, M., Stieglitz, T.: Matrix-addressable, active electrode arrays for neural stimulation using organic semiconductors-cytotoxicity and pilot experiments in vivo. *J. Neural Eng.* **5**(1), 68–74 (2008)
34. Bergveld, P., Wiersma, J., Meertens, H.: Extracellular potential recordings by means of a field effect transistor without gate metal, called OSFET. *IEEE Trans. Biomed. Eng., BME* **23**(2), 136–144 (1976)
35. Rosenfalck, P.: Intra and extracellular potential field of active nerve and muscle fibers. *Acta Physiologica Scandinavia* (1959)
36. Jobling, D.T., Smith, J.G., Wheal, H.V.: Active microelectrode array to record from the mammalian central nervous system in vitro. *Med. Biol. Eng. Comput.* **19**(5), 553–560 (1981)
37. Regehr, W.G., Pine, J., Cohan, C.S., Michelle, D.M., Tank, D.W.: Sealing cultured invertebrate neurons to embedded dish electrodes facilitates long-term stimulation and recording. *J. Neurosci. Methods* **30**, 91–106 (1989)
38. Fromherz, P., Offenhausser, A., Vetter, T., Weis, J.: A neuron-silicon junction: a retzius cell of the leech on an insulated-gate field-effect transistor. *Science* **252** (1991)
39. Fromherz, P.: Neuroelectronic interfacing: semiconductor chips with ion channels, nerve cells, and brain. *Nanoelectron. Inf. Technol.* **129**, 781–810 (2003)
40. Kaul, R., Syed, N., Fromherz, P.: Neuron-semiconductor chip with chemical synapse between identified neurons. *Phys. Rev. Lett.* **92**(3), 1–4 (2004)
41. Hutzler, M., Fromherz, P.: Silicon chip with capacitors and transistors for interfacing organotypic brain slice of rat hippocampus. *Neuroscience* **19**, 2004 (2003)
42. Vassanelli, S., Fromherz, P.: Transistor probes local potassium conductances in the adhesion region of cultured rat hippocampal neurons. *J. Neurosci.: Off. J. Soc. Neurosci.* **19**(16), 6767–6773 (1999)
43. Fromherz, P.: Joining microelectronics and microionics: nerve cells and brain tissue on semiconductor chips. *Solid-State Electron.* **52**(9), 1364–1373 (2008)
44. Fromherz, P.: Electrical interfacing of nerve cells and semiconductor chips. *Chemphyschem: Eur. J. Chem. Phys. Phys. Chem.* **3**(3), 276–284 (2002)
45. Schätzthauer, R., Fromherz, P.: Neuron-silicon junction with voltage-gated ionic currents. *Eur. J. Neurosci.* **10**(6), 1956–1962 (1998)
46. Weis, R., Müller, B., Fromherz, P.: Neuron adhesion on a silicon chip probed by an array of field-effect transistors. *Phys. Rev. Lett.* **76**(2), 327–330 (1996)
47. Fromherz, P.: Semiconductor chips with ion channels, nerve cells and brain. *Physi. E: Low-dimens. Syst. Nanostruct.* **16**(1), 24–34 (2003)
48. Vassanelli, S., Fromherz, P.: Neurons from rat brain coupled to transistors. *Appl. Phys. A: Mater. Sci. Process.* **65**(2), 85–88 (1997)
49. Stett, A., Müller, B., Fromherz, P.: Two-way silicon-neuron interface by electrical induction. *Phys. Rev. E* **55**(2), 1779–1782 (1997)
50. Ulbrich, M., Fromherz, P.: Neuron-silicon self-excitation: a prototype of iono-electronics. *Adv. Mater.* **13**(5), 344–347 (2001)
51. Maher, M.P., Pine, J., Wright, J., Tai, Y.C.: The neurochip: a new multielectrode device for stimulating and recording from cultured neurons. *J. Neurosci. Methods* **87**(1), 45–56 (1999)
52. Jing, G., Yao, Y., Gnerlich, M., Perry, S., Tatic-Lucic, S.: Towards a multi-electrode array (MEA) system for patterned neural networks. *Procedia Chem.* **1**(1), 329–332 (2009)
53. Dworak, B.J., Wheeler, B.C.: Novel MEA platform with PDMS microtunnels enables the detection of action potential propagation from isolated axons in culture. *Lab on a chip* (2009)
54. Scharifker, B.: Diffusion to ensembles of microelectrodes. *J. Electroanal. Chem. Interfacial Electrochem.* **240**(1–2), 61–76 (1988)
55. Wise, K.D.: Silicon microsystems for neuroscience and neural prostheses. *IEEE Eng. Med. Biol. Mag.* **24**(5), 22–29 (2005)
56. Heer, F., Hafizovic, S., Ugniwenko, T., Frey, U., Franks, W., Perriard, E., Perriard, J.-C., Blau, A., Ziegler, C., Hierlemann, A.: Single-chip microelectronic system to interface with living cells. *Biosens. Bioelectron.* **22**(11), 2546–2553 (2007)

57. Willemin, M.: Optical characterization methods for solid-state image sensors. *Optics Lasers Eng.* **36**(2), 185–194 (2001)
58. Berdondini, L., van der Wal, P.D., Guenat, O., de Rooij, N.F., Koudelka-Hep, M., Seitz, P., Kaufmann, R., Metzler, P., Blanc, N., Rohr, S.: High-density electrode array for imaging in vitro electrophysiological activity. *Biosens. Bioelectron.* **21**(1), 167–174 (2005)
59. Berdondini, L., Imfeld, K., Maccione, A., Tedesco, M., Neukom, S., Koudelka-Hep, M., Martinioia, S.: Active pixel sensor array for high spatio-temporal resolution electrophysiological recordings from single cell to large scale neuronal networks. *Lab Chip* **9**(18), 2644–2651 (2009)
60. Krause, M.: Extended gate electrode arrays for extracellular signal recordings. *Sens. Actuators B: Chem.* **70**(1–3), 101–107 (2000)
61. Ecken, H., Ingebrandt, S., Krause, M., Richter, D., Hara, M., Offenhäusser, A.: 64-Channel extended gate electrode arrays for extracellular signal recording. *Electrochim. Acta* **48**(20–22), 3355–3362 (2003)
62. Meyburg, Sven, Goryll, Michael, Moers, Jürgen, Ingebrandt, Sven, Böcker-Meffert, Simone, Lüth, Hans, Offenhäusser, Andreas: N-Channel field-effect transistors with floating gates for extracellular recordings. *Biosens. Bioelectron.* **21**(7), 1037–1044 (2006)
63. Cohen, A., Spira, M.E., Yitshaik, S., Borghs, G., Schwartzglass, O., Shappir, J.: Depletion type floating gate p-channel MOS transistor for recording action potentials generated by cultured neurons. *Biosens. Bioelectron.* **19**(12), 1703–1709 (2004)

Organic Transistor Devices for In Vitro
Electrophysiological Applications

Spanu, A.

2016, XIV, 120 p. 82 illus., 62 illus. in color., Hardcover

ISBN: 978-3-319-28879-6